Table of Content

R=H, CH₃, Br, NO₂   R'=H, CH₃, Cl,......   Cat.=Fe₃O₄@SiO₂@(NH₄)₆Mo₇O₂₄   12 examples   up to 95.2% isolated yield

An eco-friendly method was developed for the synthesis of 2-benzimidazoles over an Fe₃O₄@SiO₂@(NH₄)₆Mo₇O₂₄ magnetic core-shell nanocomposite using hydrogen peroxide.

An ammonium molybdate deposited amorphous silica coated iron oxide magnetic core-shell nanocomposite for the efficient synthesis of 2-benzimidazoles using hydrogen peroxide

Guoyi Bai[*], Xingwang Lan, Xiaofang Liu, Chen Liu, Lingjuan Shi, Qingzhi Chen, and Guofeng Chen

An ammonium molybdate deposited amorphous silica coated iron oxide ($Fe_3O_4@SiO_2$) magnetic core-shell nanocomposite was prepared and tested in the application to the synthesis of 2-benzimidazoles from aromatic aldehydes and *o*-phenylenediamines using hydrogen peroxide as an oxidant at room temperature. It was found that the yields were fundamentally influenced by the nature and position of the substituents on the phenyl ring. Brunauer-Emmett-Teller (BET), X-ray diffraction (XRD), transmission electron microscope (TEM), energy-dispersive X-ray (EDX), and X-ray photoelectron spectroscopy (XPS) characterizations confirmed that the active ammonium molybdate species are highly dispersed on the surface of the $Fe_3O_4@SiO_2$ magnetic core-shell nanocomposite, accounting for its good activity. A method was eventually developed for the synthesis of 2-benzimidazoles highlighting the good activity and easily-recyclable nature of this magnetic catalyst.

Introduction

2-Benzimidazole and its derivates are important aromatic nitrogen heterocycles due to their ubiquitous presence and wide applications in many pharmaceutical and biological areas including antiulcer agents, antihypertensives, antivirals, antifungals, anticancers, and antihistaminics, as well as in organic synthesis.[1-6] The widespread interest in 2-benzimidazoles has prompted extensive studies for their synthesis and a series of methods has been subsequently developed during recent decades. The coupling of *o*-phenylenediamines with carboxylic acids[7] or their derivates[8] is an established general method to prepare benzimidazoles, but the harsh reaction conditions and relatively low yields limit applications. Alternatively, the oxidative cyclodehydrogenation of aniline Schiff bases, generated *in situ* from the condensation of *o*-phenylenediamines with aldehydes,[9] over various oxidants or catalysts has become popular due to the high efficiency and green nature of this approach. The generally employed oxidants or catalysts include $In(OTf)_3$,[10] $FeCl_3$,[11] DDQ,[12] I_2,[13] NH_4OAc,[14] SDS,[15] IBD,[16] DMP,[17] $NaHSO_3$,[18] $Na_2S_2O_5$,[19] Scolecite,[20] Dowex 50W,[21] H_2O_2/HCl,[22] H_2O_2/Bu_4NI,[23] H_2O_2/CAN.[24] The application of these reagents has resulted in the efficient synthesis of benzimidazoles, but some procedures still have problems such as the use of toxic or precious metallic catalysts, and the difficulties in catalyst recycling. These problems have limited the practical applications of this approach and there has been great demand for the application of a green oxidant and a recyclable catalyst for the synthesis of benzimidazoles.

On the other hand, polyoxometalates have been widely used as homogeneous or heterogeneous catalysts in organic synthesis due to their excellent catalytic activity, good solubility, and non-toxicity.[25-29] For instance, Iraj *et al.*[28] have reported the synthesis of various oxazolines and imidazolines over tungstophosphoric acid, and excellent yields were achieved in a short time. Autino *et al.*[29] have obtained good results under solvent-free conditions in the synthesis of substituted coumarins from phenols and β-ketoesters over Wells-Dawson

polyoxometalates. However, the difficulty in efficient recycling of the used polyoxometalates has limited their further application, mainly ascribed to their high solubility in water. Thus, preparation and application of supported polyoxometalates have attracted much attention in recent years.[30, 31] For example, García-Gutierrez *et al.*[31] have developed an efficient γ-Al_2O_3 supported ammonium molybdate catalyst for the ultra-deep oxidative desulfurization of diesel fuel using hydrogen peroxide as an oxidant. Recently, magnetic core-shell nanocomposites are becoming popular as a novel supported catalyst due to their chemically modifiable surface, magnetically separable nature and good stability.[32-34] For instance, Wu *et al.*[33] have reported a magnetically separable $Fe_3O_4@SiO_2@Pd$-Au nanocomposite for the liquid-phase hydrodechlorination of 4-chlorophenol under mild conditions, exhibiting an excellent catalytic performance. An *et al.*[34] have prepared a novel $Fe_3O_4@SiO_2@AgCl$:Ag nanocomposite via visible-light reduction method and tested it in the decomposition of organic pollutants. This catalyst can be effectively recycled for many times without loss of its activity. However, to the best of our knowledge, no work on the synthesis of 2-benzimidazoles over core-shell structured nanocomposites has been reported.

In a continuation of our previous work,[35] we herein report our recent research into the green and efficient synthesis of 2-benzimidazoles from aromatic aldehydes and *o*-phenylenediamines via a hydrogen peroxide oxidation system involving a novel ammonium molybdate deposited $Fe_3O_4@SiO_2$ magnetic core-shell nanocomposite ($Fe_3O_4@SiO_2@(NH_4)_6Mo_7O_{24}$). This catalyst exhibits good catalytic performance in the synthesis of 2-benzimidazoles and can be easily recycled. The mechanism of this transformation will be discussed in this paper and the structure of this core-shell nanocomposite has been confirmed.
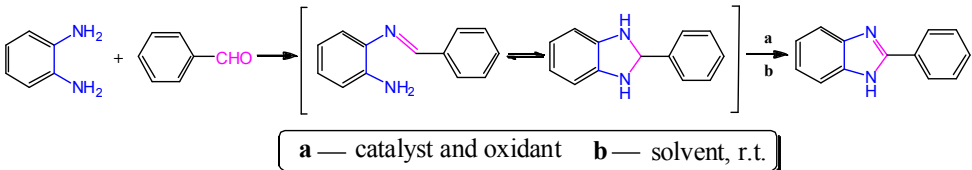
Results and discussion

Initially, the synthesis of 2-phenylbenzimidazole as a representative 2-benzimidazole, from benzaldehyde and *o*-phenylenediamine, was carried out over different hydrogen

peroxide and polyoxometalates or surfactant combinations, and the results are listed in Table 1. As can be seen, the selectivity for 2-phenylbenzimidazole was only 48.3%, together with formation of appreciable quantities of Schiff base intermediates, in the absence of a catalyst. Gratifyingly, among the catalysts studied, ammonium molybdate was found to markedly improve the selectivity of 2-phenylbenzimidazole, achieving 97.7% in 180 min; much higher than other catalysts. On the other hand, 2-phenylbenzimidazole was obtained in 48.7% selectivity in the presence of air without any hydrogen peroxide; whereas, it decreased to 14.4% in the absence of both hydrogen peroxide and air (Table 1, entries 8 and 9), indicating that ammonium

molybdate itself has poor catalytic activity. Therefore, we speculated that peroxomolybdate intermediates or other peroxides, generated from ammonium molybdate with hydrogen peroxide and air, account for the high activity of this catalytic system. Furthermore, we also examined the effect of reaction time. It was found that, although the conversion still remained at a high level, the selectivity for 2-phenylbenzimidazole decreased dramatically from 97.7% to 17.4% with the reaction time decreased from 180 min to 60 min; whereas, it was nearly unchanged when the reaction time was prolonged from 180 min to 240 min. Thus, 180 min is regarded as an appropriate reaction time for this catalytic system.

Table 1

Effect of different catalytic systems on the synthesis of 2-phenylbenzimidazole.[a]

a — catalyst and oxidant   **b** — solvent, r.t.

Entry	Oxidant	Catalyst	Time (min)	Conversion (%)[b]	Selectivity (%)[b]
1	H_2O_2	-	180	93.2	48.3
2	H_2O_2	$H_3PW_{12}O_{40}$	180	95.4	64.9
3	H_2O_2	Na_2WO_4	180	96.0	20.3
4	H_2O_2	Na_2MoO_4	180	98.0	71.6
5	H_2O_2	$(NH_4)_6Mo_7O_{24}$	180	94.1	97.7
6	H_2O_2	TBAB	180	92.4	38.4
7	H_2O_2	CTAB	180	98.4	29.2
8	-	$(NH_4)_6Mo_7O_{24}$	180	98.3	48.7
9	-	$(NH_4)_6Mo_7O_{24}$[c]	180	96.2	14.4
10	H_2O_2	$(NH_4)_6Mo_7O_{24}$	120	96.7	62.1
11	H_2O_2	$(NH_4)_6Mo_7O_{24}$	60	97.9	17.4
12	H_2O_2	$(NH_4)_6Mo_7O_{24}$	240	93.5	94.4

[a] Reaction conditions: benzaldehyde (1.0 mmol), *o*-phenylendiamine (1.1 mmol), EtOH (5.0 mL), catalyst (0.04 mmol), H_2O_2 (0.2 mL). [b] Determined by HPLC based on the starting material. [c] Operated under a nitrogen atmosphere.   TBAB = tetrabutyl ammonium bromide. CTAB = cetyl trimethyl ammonium bromide.

To solve the difficulty of efficient recycling of the used ammonium molybdate and shorten the reaction time, we proposed to prepare a new supported ammonium molybdate catalyst. Considering that magnetic separation is more attractive and efficient than traditional filtration or centrifugation, we decided to immobilize ammonium molybdate on a $Fe_3O_4@SiO_2$
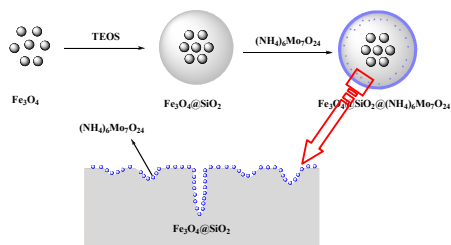

Figure 1. Stepwise preparation of $Fe_3O_4@SiO_2@(NH_4)_6Mo_7O_{24}$ magnetic core-shell nanocomposite.

magnetic core-shell nanocomposite by combining the Stöber and the equilibrium adsorption methodology, as illustrated in Figure 1. Thus, a novel $Fe_3O_4@SiO_2@(NH_4)_6Mo_7O_{24}$ catalyst was first prepared and applied to the synthesis of 2-benzimidazoles (Table 2).

As envisaged, the $Fe_3O_4@SiO_2@(NH_4)_6Mo_7O_{24}$ catalyst could be effectively separated from the reaction mixture by an external magnetic field after the completion of reaction. Of note, the selectivity for 2-phenylbenzimidazole increased markedly to 94.0% in 30 min; whereas, it was only 11.9% over the unsupported ammonium molybdate, 11.6% in the absence of any catalyst and 18.3% over $Fe_3O_4@SiO_2$. On the other hand, the conversion of benzaldehyde was only 81.0% when catalyzed by ammonium molybdate directly immobilized on Fe_3O_4 ($Fe_3O_4@(NH_4)_6Mo_7O_{24}$) by the same method, although the selectivity for 2-phenylbenzimidazole was similar. Thus, it appears that supporting ammonium molybdate on $Fe_3O_4@SiO_2$ not only solves the problem of separation of ammonium molybdate from the reaction mixture but also improves the dispersion of the active ammonium molybdate on the surface of

SiO_2, accounting for the high activity of $Fe_3O_4@SiO_2@(NH_4)_6Mo_7O_{24}$.

Furthermore, the effect of solvents was also investigated under the same reaction conditions (Table 2). It became apparent that the conversion of benzaldehyde decreased in other solvents compared to ethanol. Considering that application of ultrasound often can reduce reaction time dramatically,[35] this reaction was also carried out under ultrasound but we only observed a slight increase on the conversion and selectivity. Thus, $Fe_3O_4@SiO_2@(NH_4)_6Mo_7O_{24}$ was finally chosen as the catalyst of choice for the synthesis of 2-phenylbenzimidazoles in ethanol as the solvent of choice.

Table 2

Effect of ammonium molybdate supported on $Fe_3O_4@SiO_2$ on the synthesis of 2-phenylbenzimidazole.[a]

Entry	Catalyst	Solvent	Conversion (%)[c]	Selectivity (%)[c]
1	Catalyst-free	EtOH	95.2	11.6
2	$(NH_4)_6Mo_7O_{24}$	EtOH	96.2	11.9
3	$Fe_3O_4@SiO_2$	EtOH	87.3	18.3
4	$Fe_3O_4@SiO_2@(NH_4)_6Mo_7O_{24}$	EtOH	92.0	94.0
5	$Fe_3O_4@(NH_4)_6Mo_7O_{24}$	EtOH	81.0	97.1
6	$Fe_3O_4@SiO_2@(NH_4)_6Mo_7O_{24}$	Solvent-free	71.8	94.7
7	$Fe_3O_4@SiO_2@(NH_4)_6Mo_7O_{24}$	H_2O	47.1	86.2
8	$Fe_3O_4@SiO_2@(NH_4)_6Mo_7O_{24}$[b]	EtOH	92.6	96.8

[a] Reaction conditions: benzaldehyde (1.0 mmol), *o*-phenylendiamine (1.1 mmol), solvent (5.0 mL), catalyst (0.22 g, including 0.04 mmol $(NH_4)_6Mo_7O_{24}$), H_2O_2 (0.2 mL), 30 min at room temperature. [b] Ultrasound heating 30 min at room temperature. [c] Determined by HPLC based on the starting material.

In addition, the stability of $Fe_3O_4@SiO_2@(NH_4)_6Mo_7O_{24}$ was investigated. The recovered $Fe_3O_4@SiO_2@(NH_4)_6Mo_7O_{24}$ was easily separated with an external magnet after reaction and then recycled under the same reaction conditions. The results depicted in Figure 2 show that $Fe_3O_4@SiO_2@(NH_4)_6Mo_7O_{24}$ can be recycled five times without appreciable loss of its catalytic activity, demonstrating its good stability as a catalyst for the synthesis of 2-phenylbenzimidazole. Further inductively coupled plasma (ICP) analysis revealed that the amount of Mo in the supernatant after the reaction is very low and nearly negligible, indicating that there is almost no loss of the ammonium molybdate active species during the recycle and in agreement with the stability results.
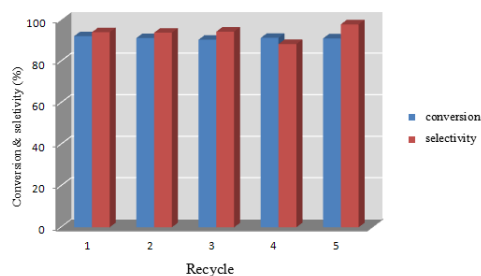

Figure 2. Reusability studies of $Fe_3O_4@SiO_2@(NH_4)_6Mo_7O_{24}$ on the synthesis of 2-phenylbenzimidazole. Reaction conditions: benzaldehyde (1.0 mmol), *o*-phenylendiamine (1.1 mmol), EtOH (5 mL), catalyst (0.22 g, including 0.04 mmol $(NH_4)_6Mo_7O_{24}$), H_2O_2 (0.2 mL) at room temperature.

Catalyst characterization

The physicochemical properties of ammonium molybdate and the magnetic core-shell nanocomposites were measured and selected results are summarized in Table 3. ICP result indicated the Mo content of $Fe_3O_4@SiO_2@(NH_4)_6Mo_7O_{24}$ was 10.0%, in agreement with the actual loading amount of ammonium molybdate. The surface area and pore volume of $Fe_3O_4@SiO_2@(NH_4)_6Mo_7O_{24}$ were higher than those of ammonium molybdate, but much lower than those of $Fe_3O_4@SiO_2$, probably owing to the active ammonium molybdate species present in the pores and assembled on its surface.

Table 3

Selected physicochemical properties of ammonium molybdate and the magnetic core-shell nanocomposites.

Sample	Mo loading (wt %)[a]	Surface area (m²/g)	Pore volume (10^{-2} cm³/g)
$(NH_4)_6Mo_7O_{24}$	-	3.4	1.1
$Fe_3O_4@SiO_2$	-	27.5	5.8
$Fe_3O_4@SiO_2@$ $(NH_4)_6Mo_7O_{24}$	10.0	8.3	2.4

[a] Based on ICP results.

Figure 3 shows X-ray diffraction (XRD) patterns of ammonium molybdate and the corresponding magnetic core-shell nanocomposites. The characteristic diffraction peaks of ammonium molybdate appear around 12.5°, 25.1°, 37.3° and 41.4°, confirming the presence of crystalline ammonium molybdate.[36] $Fe_3O_4@SiO_2$ shows characteristic diffraction peaks at about 30.4°, 35.8°, 43.5°, 53.5°, 57.6° and 63.3°, just like those of pure Fe_3O_4 (JCPDS: 00-003-0862), indicating that the embedded Fe_3O_4 retains its crystalline structure after SiO_2 coating, while the SiO_2 exists in an amorphous state. However, the diffraction peaks of $Fe_3O_4@SiO_2@(NH_4)_6Mo_7O_{24}$ are similar to those of $Fe_3O_4@SiO_2$ with no characteristic diffraction peaks corresponding to ammonium molybdate being observed, indicating that the active ammonium molybdate species either exists in an amorphous state or highly dispersed on the surface and in the pores of $Fe_3O_4@SiO_2$. Selected-area electron diffraction (SAED) patterns obtained from the shell edges of $Fe_3O_4@SiO_2@(NH_4)_6Mo_7O_{24}$ are characterized by broken

diffraction rings (inset in Figure 3), demonstrating the crystalline structure of Fe_3O_4 in $Fe_3O_4@SiO_2@(NH_4)_6Mo_7O_{24}$, in accordance with the XRD results.
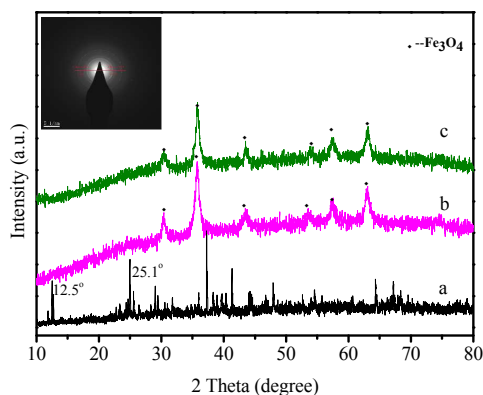
Figure 3. XRD patterns of $(NH_4)_6Mo_7O_{24}$ and the core-shell nanocomposites. (a) $(NH_4)_6Mo_7O_{24}$, (b) $Fe_3O_4@SiO_2$, (c) $Fe_3O_4@SiO_2@(NH_4)_6Mo_7O_{24}$. The inset is the SAED image of $Fe_3O_4@SiO_2@(NH_4)_6Mo_7O_{24}$.

The nitrogen adsorption-desorption isotherms and the pore size distribution curves of $Fe_3O_4@SiO_2$ and $Fe_3O_4@SiO_2@(NH_4)_6Mo_7O_{24}$ are shown in Figure 4. The nitrogen sorption isotherms of both magnetic core-shell nanocomposites resembled typical type IV isotherms[37] together with a hysteresis loop of type H3 in the P/P_0 range of 0.4-1.0, arising from capillary condensation. The pore size distribution curve of $Fe_3O_4@SiO_2$ showed a sharp peak at 3.9 nm and fluctuations between 5-40 nm (inset), which might be due to the micropores nature and interstices between the primary particles, improving the adsorption ability of $Fe_3O_4@SiO_2$; whereas, the pore size distribution curve of $Fe_3O_4@SiO_2@(NH_4)_6Mo_7O_{24}$ merely fluctuated over a wide range, indicating only interstices between the primary particles.[38] Thus, we speculate that the active ammonium molybdate species are deposited on the $Fe_3O_4@SiO_2$ magnetic core-shell nanocomposite, obstructing the micropores and some interstices, in agreement with its smaller BET surface area and pore volume.
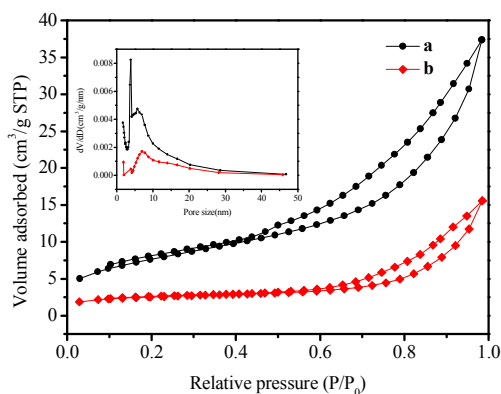
Figure 4. Nitrogen adsorption-desorption isotherms and the pore size distributions (the inset) of the core-shell nanocomposites (a) $Fe_3O_4@SiO_2$ and (b) $Fe_3O_4@SiO_2@(NH_4)_6Mo_7O_{24}$.

The surface morphology and the particle distributions of the corresponding magnetic core-shell nanocomposites were recorded by transmission electron microscope (TEM) and high resolution transmission electron microscope (HRTEM). From Figure 5 a and b, it can be seen that each nanocomposite contains several uniform spherical shape Fe_3O_4 nanoparticles (approximate 6 nm in diameter) in one SiO_2 shell. The existence of the ammonium molybdate species on the surface of $Fe_3O_4@SiO_2$ nanocomposites was difficult to confirm from the TEM and HRTEM investigations (Figure 5 c and d), indicating that the ammonium molybdate species were highly dispersed on the surface or pores and not in a crystalline state. Further analysis on particle distributions showed that $Fe_3O_4@SiO_2@(NH_4)_6Mo_7O_{24}$ has a little larger average particle size (approximate 62 nm) than $Fe_3O_4@SiO_2$ (approximate 58 nm) (Figure 5, inset a and c), although both of them intend to form larger aggregates due to the magnetic nature of Fe_3O_4. This suggests that the active ammonium molybdate species might assemble on the surface of $Fe_3O_4@SiO_2$ to form a monolayer, in agreement with the scanning electron microscopy (SEM) and energy dispersive X-ray (EDX) results (Figure S1 and S2).

Scanning transmission electron microscope (STEM) images of $Fe_3O_4@SiO_2@(NH_4)_6Mo_7O_{24}$ are depicted in Figure 6, together with a representative high-angle annular dark-field (HAADF) image and elemental mapping of the nanocomposite. The results demonstrate the presence of the expected molybdenum in the structure of this nanocomposite, as confirmed by the mapping of the related Si, Fe and O elements (Figure 6 c-g). The distribution of the molybdenum supports our previous assumption that the ammonium molybdate species were highly dispersed on the surface and in the pores of $Fe_3O_4@SiO_2$ nanocomposites.
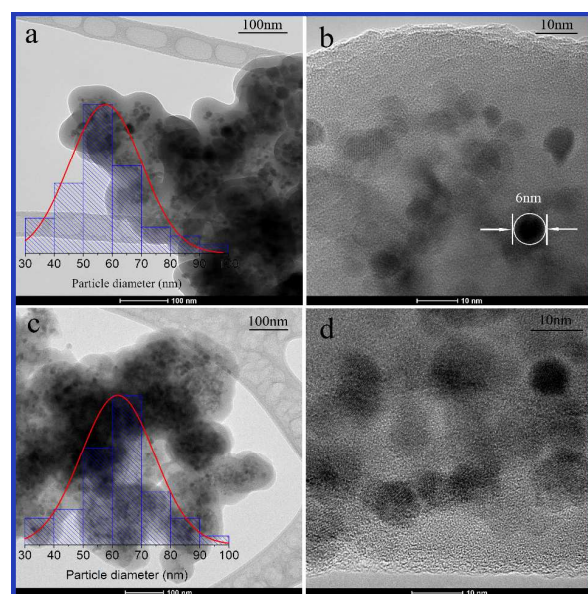

Figure 5. TEM and HRTEM images of (a and b) $Fe_3O_4@SiO_2$ and (c and d) $Fe_3O_4@SiO_2@(NH_4)_6Mo_7O_{24}$ nanocomposites. (Inset a and c: the particle distributions of $Fe_3O_4@SiO_2$ and $Fe_3O_4@SiO_2@(NH_4)_6Mo_7O_{24}$).
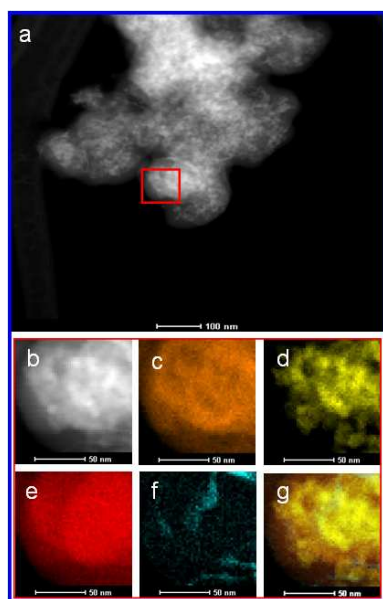
Figure 6. (a) STEM image of $Fe_3O_4@SiO_2@(NH_4)_6Mo_7O_{24}$. (b) HAADF-STEM image of $Fe_3O_4@SiO_2@(NH_4)_6Mo_7O_{24}$, with elemental mapping of (c) Si, (d) Fe, (e) O, (f) Mo, and (g) their overlap shown in the bottom row.

X-ray photoelectron spectroscopy (XPS) spectra of $Fe_3O_4@SiO_2$ and $Fe_3O_4@SiO_2@(NH_4)_6Mo_7O_{24}$ are shown in Figure 7. It was found that no Fe element was detected on the surface of either nanocomposites, demonstrating that the Fe_3O_4 nanoparticles were well coated by the pyknotic SiO_2 shell. Furthermore, two peaks related to Mo $3d_{5/2}$ and Mo $3d_{3/2}$ (inset) could be observed on the surface of $Fe_3O_4@SiO_2@(NH_4)_6Mo_7O_{24}$. Their binding energies are 232.7 and 235.8 eV respectively, suggesting the presence of $(Mo_7O_{24})^{6-}$ structure, as also reported in previous literature.[39] Further thermogravimetric (TG) and differential thermogravimetric (DTG) measurements (Figure S3) confirmed that $Fe_3O_4@SiO_2@(NH_4)_6Mo_7O_{24}$ is relatively stable within 473 K; whereas, $(NH_4)_6Mo_7O_{24}\cdot4H_2O$ will only lose its crystaline water during the preparation process, in agreement with the above XPS results.
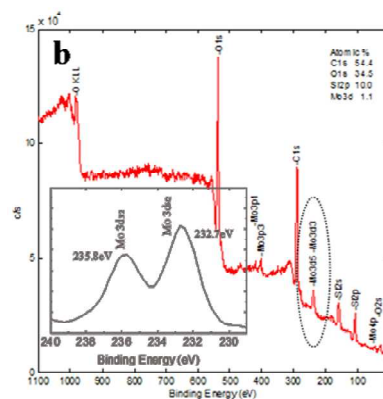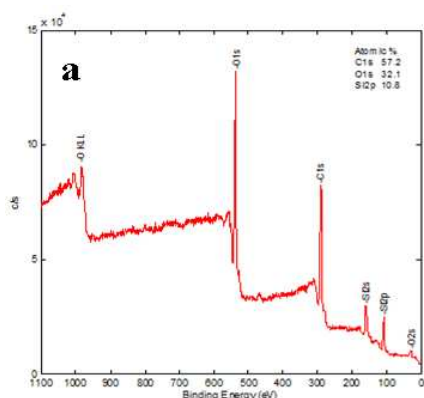
Figure 7. XPS spectra of (a) $Fe_3O_4@SiO_2$ and (b) $Fe_3O_4@SiO_2@$ $(NH_4)_6Mo_7O_{24}$ nanocomposites. Inset (b) is the high resolution XPS spectra of Mo element in $Fe_3O_4@SiO_2@(NH_4)_6Mo_7O_{24}$.

The room temperature hysteresis loops of $Fe_3O_4@SiO_2$ and $Fe_3O_4@SiO_2@(NH_4)_6Mo_7O_{24}$ nanocomposites are shown in Figure 8. As can be seen, the saturation magnetization (Ms) value of $Fe_3O_4@SiO_2$ is 37.6 emu/g at an applied field of 20000 Oe; whereas, the Ms value of $Fe_3O_4@SiO_2@(NH_4)_6Mo_7O_{24}$ decreases to 28.0 emu/g, ascribed to the deposition of $(NH_4)_6Mo_7O_{24}$ on the surface of $Fe_3O_4@SiO_2$. Moreover, the magnetization curves showed no remanence or coercivity in both samples, suggesting their superparamagnetic character.[40] Thus, the $Fe_3O_4@SiO_2@(NH_4)_6Mo_7O_{24}$ nanocomposites can be easily separated from the reaction mixture by an external magnetic field (inset in Figure 8), but the pure ammonium molybdate cannot.
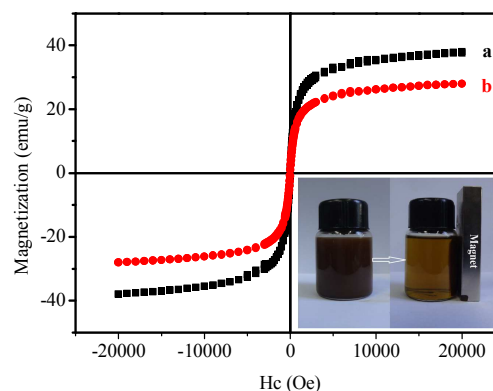

Figure 8. Room temperature hysteresis loops of the core-shell nanocomposites. (a) $Fe_3O_4@SiO_2$ and (b) $Fe_3O_4@SiO_2@(NH_4)_6Mo_7O_{24}$. Inset is photographs of $Fe_3O_4@SiO_2@(NH_4)_6Mo_7O_{24}$ before (left) and after (right) magnetic separation by an external magnetic field.

Speculation of reaction mechanism

A plausible mechanism of this reaction is proposed based on the experimental results and previous literature observations,[23, 24, 31] as shown in Scheme 1. Intermediate **2** is initially formed via cyclization of Schiff base intermediate **1**, which is formed by rapid condensation from benzaldehyde and *o*-phenylenediamine in the absence of catalyst, as Zhu[23] and Bahrami[24] have described. Then, the intermediate **2** reacts with the *in situ*

generated peroxomolybdate intermediates **6**,[31] from the oxidation of the supported molybdate species **5** by hydrogen peroxide, to afford the key intermediate **3**, together with the regeneration of **5** and irreversible loss of water. Finally, the rapid

oxidative dehydrogenation of intermediate **3** generates the desired 2-phenylbenzimidazole.[41]
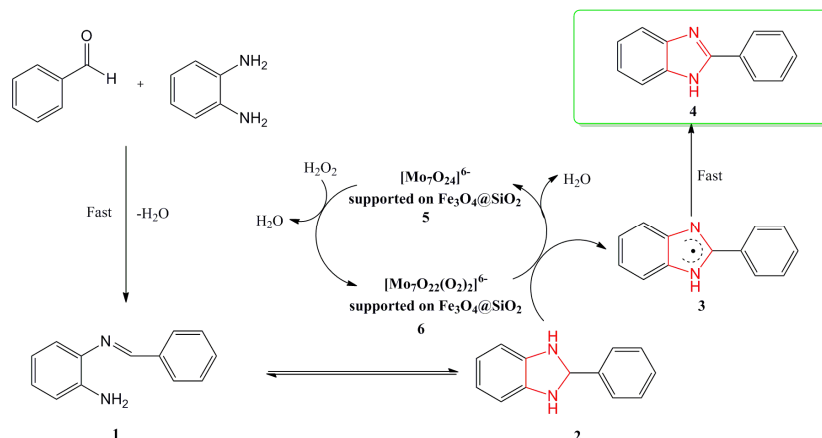
Scheme 1. A plausible mechanism for the synthesis of 2-phenylbenzimidazole.

Synthesis of derivates

To evaluate the versatility of this method, a series of aromatic aldehydes was then examined with *o*-phenylenediamines under the optimum reaction conditions, as shown in Table 4. In all cases, the reaction was carried out over periods of 30 min to 65 min. All products were characterized by FT-IR, ^{1}H NMR, ^{13}C NMR and HRMS spectroscopy. As expected, all aromatic aldehydes reacted smoothly with *o*-phenylenediamine to provide the corresponding 2-benzimidazoles in good to excellent isolated yields. Furthermore, reactions of the *p*-substituted aldehydes possessing electron-withdrawing groups, such as -Cl, -NO$_2$, underwent much faster reaction than those possessing electron-donating groups, such as -OCH$_3$, -OH, suggesting that the electron-withdrawing groups are favorable for this transformation. In contrast, comparing the reaction results of substituted benzaldehydes with the -Cl group in various positions, the steric factors of the substituents are proven to have less influence on the reaction rate. Thus, we can conclude that electronic factors are the main controlling effect in this transformation rather than steric factors. Moreover, the reaction of benzaldehyde with some substituted *o*-phenylenediamines also gave the corresponding 2-benzimidazoles smoothly in excellent yields, indicating the wide versatility of this method.

Conclusions

In summary, we have developed a green and efficient one-pot synthetic route to prepare 2-benzimidazoles from aldehydes and *o*-phenylenediamines using hydrogen peroxide as an oxidant at room temperature. A novel Fe$_3$O$_4$@SiO$_2$@(NH$_4$)$_6$Mo$_7$O$_{24}$ magnetic core-shell nanocomposite has been prepared and demonstrated to be a highly efficient catalyst for this transformation. It can be recycled and reused several times without any appreciable loss of its initial catalytic activity. The noteworthy advantages of this method are its high efficiency,

rapid and easy isolation of used catalyst, and green and mild reaction conditions, which make it an attractive and useful contribution to present methodologies.

Experimental section
Catalyst preparation

The Fe$_3$O$_4$@SiO$_2$@(NH$_4$)$_6$Mo$_7$O$_{24}$ magnetic core-shell nanocomposite was prepared by a combination of the Stöber and equilibrium adsorption methodology, described as follows.

The core-shell Fe$_3$O$_4$@SiO$_2$ nanocomposite was first prepared by the hydrolysis of tetraethyl orthosilicate (TEOS) on the surface of Fe$_3$O$_4$ nanoparticles in a similar manner to the protocol reported in previous literature.[42] In a typical procedure, 1.4 g Fe$_3$O$_4$ powder was first dispersed in 70 mL deionized water. An absolute ethanol solution containing 5.0 mL 25 wt% aqueous ammonia was then added to the magnetite suspension with stirring at 303 K over 15 min. After that, 4.0 mL TEOS was added slowly and the mixture was vigorously stirred for 12 h. Finally, the Fe$_3$O$_4$@SiO$_2$ was washed with absolute ethanol several times, collected by magnet, dried and then kept under vacuum for further use.
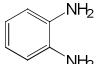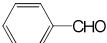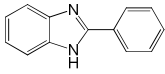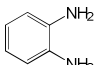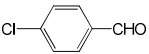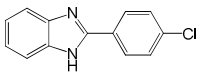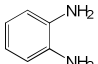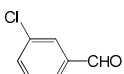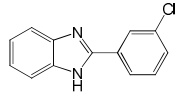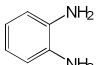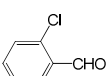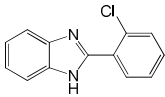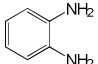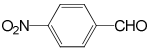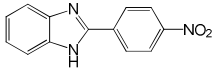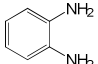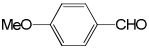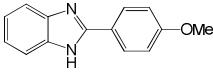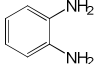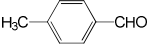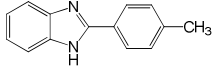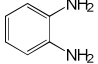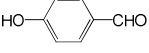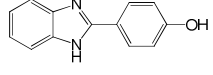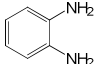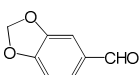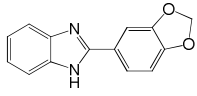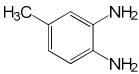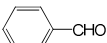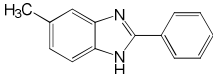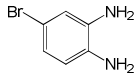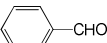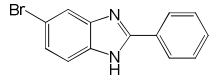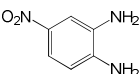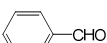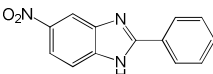
Fe$_3$O$_4$@SiO$_2$@(NH$_4$)$_6$Mo$_7$O$_{24}$ was then prepared by the following run: the prepared Fe$_3$O$_4$@SiO$_2$ nanocomposite (1.0 g) was first impregnated with an aqueous solution of 0.25 g ammonium molybdate at room temperature. The wet samples were dried at room temperature overnight and then dried at 403 K in air for 2 h. Finally, the Fe$_3$O$_4$@SiO$_2$@(NH$_4$)$_6$Mo$_7$O$_{24}$ nanocomposite thus obtained was kept under vacuum for further use.

Instruments and methods

The amount of Mo in the supernatant after the reaction was tested by ICP on an Agilent7500a spectrometer. The Mo content of the Fe$_3$O$_4$@SiO$_2$@(NH$_4$)$_6$Mo$_7$O$_{24}$ magnetic core-shell nanocomposite was identified by ICP on a Varian Vista-MPX spectrometer. BET surface areas and pore volumes of the catalysts were tested

Table 4

Synthesis of 2-benzimidazoles from aldehydes and diamines.[a]

Entry	Diamine	Aldehyde	Product	Time (min)	Yield (%)[b]
1				30	90.3
2				30	94.6
3				45	93.0
4				35	90.4
5				35	90.9
6				65	87.3
7				40	89.7
8				65	88.9
9				60	91.7
10				35	95.2
11				35	93.7
12				45	91.0

[a] Reaction conditions: aldehyde (1.0 mmol), diamine (1.1 mmol), EtOH (5.0 mL), catalyst (0.22 g, including 0.04 mmol $(NH_4)_6Mo_7O_{24}$), H_2O_2 (0.2 mL). [b] Yields of isolated products.

by nitrogen physisorption at 77 K on a Micromeritics Tristar II 3020 apparatus. Before measurements, the samples were dried at 393 K for 2 h. Powder XRD patterns were measured with a Bruker D 8 diffractometer using a Cu Kα radiation source at 40 kV and 100 mA with a step size of 0.01° 2θ over the range 10 to 80°. TEM images were acquired with a FEI Tecnai G2 F20 X-Twin microscope at extraction voltage of 3950 V, gun lens 1 and spot size 1. STEM/EDX maps were obtained at spot size 6 and diffraction pattern was acquired with a Camera Length of 300 mm. The average particle sizes were estimated on the basis of 50 particles. XPS analysis was carried out on a PHI 1600 spectrometer using monochromatic Mg Kα as the excitation source. The catalyst was mounted on the sample holder, where the background pressure was lower than 2×10^{-8} Torr. All the binding energy (BE) values were calibrated by the C 1s peak of contaminant carbon at 284.6 eV. Magnetization curves were obtained on a LDJ9600-1 Superconducting quantum interference device at room temperature.

General procedure for the synthesis of 2-benzimidazoles

A mixture of aromatic aldehydes (1.0 mmol) and o-phenylenediamines (1.1 mmol) was first stirred in ethanol (5.0 mL) at room temperature. The catalyst (0.22 g, including 0.04 mmol $(NH_4)_6Mo_7O_{24}$) and 30.0% H_2O_2 (0.2 mL) were then added into the above mixture and reacted at room temperature for the

requisite period of time while monitoring the reaction progress by TLC or HPLC. The reaction mixture was analyzed by HPLC using a BaseLine C_{18} column (150 mm × 4.6 mm) with a mobile phase of methanol/water (7:3 by volume) at a 0.6 mL/min constant flow.

After completion of the reaction, the catalyst was first separated by an external magnet for recycling and the residual reaction mixture was diluted with ethyl acetate (30.0 mL). Then, the solution was concentrated and the products were finally isolated by column chromatography on 200-300 mesh silica gel using petroleum ether: ethyl acetate = 6:1~4:1 as eluent. Analytical and spectroscopic data of the series of 2-benzimidazoles are given in the Electronic Supplementary Information.

Acknowledgments

Notes and references

^{a} *Key Laboratory of Chemical Biology of Hebei Province, College of Chemistry and Environmental Science, Hebei University, Baoding 071002, PR China*
Fax: +86-312-5937102; phone: +86-312-5079359; e-mail: baiguoyi@hotmail.com
† *Electronic Supplementary Information (ESI) available: Segmental details of the experimental procedures, the catalyst characterization results (SEM, TG, DTG, and TEM), and the spectra date of the obtained compounds (IR, NMR, and HRMS) are shown in this file.*

1 A.R. Porcari, R.V. Devivar, L.S. Kucera, J.C. Drach, L.B. Townsend, *J. Med. Chem.,* 1998, **41**, 1252.

2 W.A. Craigo, B.W. LeSueur, E.B. Skibo, *J. Med. Chem.*, 1999, **42**, 3324.

3 W. Guba, L.G. Green, R.E. Martin, O. Roche, N. Kratochwil, H. Mauser, C.Bissantz, A. Christ, M. Stahl, *J. Med. Chem.,* 2007, **50**, 6295.

4 L.J. Goossen, T. Knauber, *J. Org. Chem.,* 2008, **73**, 8631.

5 S. Gangula, C.R. Elati, A. Neredla, S.R. Baddam, U.K. Neelam, R. Bandichhor, A. Dongamanti, *Org. Process Res. Dev.,* 2010, **14**, 229.

6 M.H. Pourgholami, L.M. Khachigian, R.G. Fahmy, S. Badar, L. Wang, S. Wai, L. Chu, D.L. Morris, *Biochem. Bioph. Res. Co.,* 2010, **397**, 729.

7 C. Zhang, L.R. Zhang, N. Jiao, *Green Chem.,* 2012, **14**, 3273.

8 (a) J.S. Peng, M. Ye, C.J. Zong, F.Y. Hu, L.T. Feng, X.Y. Wang, Y.F. Wang, C.X. Chen, *J. Org. Chem.,* 2011, **76**, 716. (b) X.Q. Diao, Y.J. Wang, Y.W. Jiang, D.W. Ma, *J. Org. Chem.,* 2009, **74**, 7974. (c) M.H. Shen, T.G. Driver. *Org. Lett.,* 2008, **10**, 3367.

9 (a) S.N. Lin, L.H. Yang, *Tetrahedron Lett.,* 2005, **46**, 4315. (b) Y. Kawashita, N.Nakamichi, H. Kawabata, M. Hayashi, *Org. Lett.,* 2003, **5**, 3713.

10 R. Trivedi, S.K. De, R.A. Gibbs, *J. Mol. Catal. A: Chem.,* 2006*,* **245**, 8.

11 M.P. Singh, S. Sasmal, W. Lu, M.N. Chatterjee, *Synthesis,* 2000, **10**, 1380.

12 J.J.V. Eynde, F. Delfosse, P. Lor, Y.V. Haverbeke, *Tetrahedron,*1999, **51**, 5813.

13 P. Gogoi, D. Konwar, *Tetrahedron Lett.,* 2006, **47**, 79.

14 H. Sharghi, O. Asemani, R. Khalifeh, *Synthetic Commun.,* 2008, **38**, 1128.

15 K. Bahrami, M.M. Khodaei, A. Nejati, *Green Chem.,* 2010, **12**, 1237.

16 L.H. Du, X.P. Luo, *Synthetic Commun.,* 2010, **40**, 2880.

17 S.K. Dabhade, R.O. Bora, M. Farooqui, C.H. Gill, *Chinese Chem. Lett.,* 2009, **20**, 893.

18 T. Yamashita, S. Yamada, Y. Yamazaki, H. Tanaka, *Synthetic Commun.,* 2009, **39**, 2982.

19 N.V. Gabriel, M.D. Hermenegilda, A.C. Francisco, L.R. Ismael, V.M. Rafael, M.M. Omar, E.S. Samuel, *Bioorg. Med. Chem. Lett.,* 2006, **16**, 4169.

20 L.S. Gadekar, B.R. Arbad, M.K. Lande, *Chinese Chem. Lett.,* 2010, **21**, 1053.

21 C. Mukhopadhyay, P.K. Tapaswi, *Catal. Commun.,* 2008, **9**, 2392.

22 K. Bahrami, M.M. Khodaei, I. Kavianinia, *Synthesis,* 2007, **4**, 0547.

23 C.J. Zhu, Y.Y. Wei, *ChemSusChem,* 2011, **4**, 1082.

24 K. Bahrami, M.M. Khodaei, F. Naali, *J. Org. Chem.,* 2008, **73**, 6835.

25 (a)M. Misono, *Catal. Today*, 2005, **100**, 95. (b) M.B. Iraj, M. Majid, T. Shahram, M. Valiollah, S.F. Hojati, *Catal. Commun.,* 2008, **9**, 1153.

26 (a) T.D. Phan, M.A. Kinch, J.E. Barker, T. Ren, *Tetrahedron Lett.,* 2005, **46**, 397. (b) J. Zhang, Y. Tang, G.Y. Li, C.W. Hu, *Appl. Catal. A: Gen.,* 2005, **278**, 251.

27 (a) J. Kaur, K. Griffin, B. Harrison, I.V. Kozhevnikov, *J. Catal.,* 2002, **208**, 448. (b) G.D Yadav, N.S Asthana, V.S Kamble, *Appl. Catal. A: Gen.,* 2003, **240**, 53. (c) C. Castro, A. Corma, J. Primo, *J. Mol. Catal. A: Chem.,* 2002, **177**, 273.

28 M.B. Iraj, M. Majid, T. Shahram, M. Valiollah, S.F. Hojati, *Catal. Commun.,* 2008, **9**, 1153.

29 G.P. Romanelli, D. Bennardi, D.M. Ruiz, G. Baronetti, H.J. Thomas, J.C. Autino, *Tetrahedron Lett.,* 2004, **45**, 8935.

30 G.D. Yadav, N.S. Asthana, V.S. Kamble, *J. Catal.,* 2003, **217**, 88.

31 J.L. García-Gutierrez, G.A. Fuentes, M.E. Hernández-Terán, P. García, F. Murrieta-Guevara, F. Jiménez-Cruz, *Appl. Catal. A: Gen.,* 2008, **334**, 366.

32 (a) A.H. Lu, E.L. Salabas, F. Schth, *Angew. Chem. Int. Ed.,* 2007, **46**, 1222. (b) X.X. Ma, J.T. Wang, M. Sun, W.N. Wang, Q.H. Wu, C. Wang, Z. Wang, *Anal. Methods,* 2013, **5**, 2809. (c) F.H Chen, Q. Gao, J.Z. Ni, *Nanotechnology,* 2008, **19**, 165103. (d) H.L. Ding, Y. X. Zhang, S. Wang, J.M. Xu, S.C. Xu, G.H. Li, *Chem. Mater.,* 2012, **24**, 4572.

33 Z.J. Wu, C.X. Sun, Y. Chai, M.H. Zhang, *RSC Adv.,* 2011, **1**, 1179.

34 C.H. An, X.J. Ming, J.Z. Wang, S.T. Wang, *J. Mater. Chem.,* 2012, **22**, 5171.

35 G.Y. Bai, X.W. Lan, G.F. Chen, X.F. Liu, T.Y. Li, L.J. Shi, *Ultrason. Sonochem.,* 2014, **21**, 520.

36 L.X. Song, M. Wang, Z. Dang, F. Y. Du, *J. Phys. Chem. B,*

2010, **114**, 3404.

37 Y.H. Deng, Y. Cai, Z.K. Sun, J. Liu, C. Liu, J. Wei, W. Li, C. Liu, Y. Wang, D.Y. Zhao, *J. Am. Chem. Soc.,* 2010, **132**, 8466.

38 X.J. Du, D.S. Zhang, R.H. Gao, L. Huang, L.Y. Shi, J.P. Zhang, *Chem. Commun.,* 2013, **49**, 6770.

39 G. Ilangovan, K.C. Pillai, *Langmuir,* 1997, **13**, 566.

40 (a) KJ. Yu, X.B. Zhang, H.W. Tong, X.Y. Yan, S.M. Liu, *Mater. Lett.,* 2013, **106**, 151. (b) X.Q. Liu, Z.Y. Ma, J.M. Xing, H.Z. Liu, *J. Magn. Magn. Mater.,* 2004**, 270**, 1.

41 H. Sharghi, M. Aberi, M.M. Doroodmand, *Adv. Synth. Catal.,* 2008, **350**, 2380.

42 G.Y. Bai, L.J. Shi, Z. Zhao, Y.L. Wang, M.D. Qiu, H.X. Dong, *Mater. Lett.,* 2013, **96,** 93.

Green Chemistry Accepted Manuscript